EPS-HEP99
Abstract # 1-384
Parallel sessions: 1,5
Plenary sessions: 1,5
ALEPH 99-059
CONF 99-034
July 7, 1999

P R E L I M I N A R Y

Investigations on the *b*-Quark Mass from Hadronic Z Decays

The ALEPH Collaboration

Contact person : G. Dissertori, Guenther.Dissertori@cern.ch

Abstract

Moments of event shape variables as well as the three-jet rate (Durham algorithm) are measured in hadronic Z decays from data taken with the ALEPH detector at LEP1 in 1994, and the ratio of the results found in *b*- and *uds*-tagged events is computed. Taking optimal variables with respect to the size of the higher order and hadronization corrections, a next-to-leading order prediction including mass effects is fitted to the measured ratios to give a value for the mass of the *b*-quark.

Contribution by ALEPH to the 1999 summer conferences

1 Introduction

The recent advent of next-to-leading order (NLO) calculations for e^+e^- annihilation into quark pairs, which take full account of quark mass effects [1, 2, 3, 4], have opened up the possibility for further tests of QCD, such as measurements of the flavour independence of the strong coupling constant [5, 7, 8] or measurements of the running b-quark mass at the M_Z scale [5, 6]. The b-quark mass is one of the fundamental parameters of the Standard Model Lagrangian, and can in principle be viewed as a parameter similar to the couplings. The renormalization procedure leads then to the definition of a running quantity, i.e., a renormalized b-quark mass which is a function of the renormalization scale. An interpretation as a particle mass is difficult because of the fact that quarks are not asymptotically free states. Nevertheless, a definition of the mass as the pole of the quark propagator is used frequently, which depending on the size of long-distance QCD effects can be viewed as the mass of an (almost) free particle.

Most of the b-quark mass determinations have been performed at rather low scales [9]. It is therefore interesting to measure this parameter at large scales within a clean environment, which is exactly the situation offered by LEP. Previous measurements have used the calculations for the ratio of three-jet rates in b- and uds-quark decays of the Z boson. For a running b-quark mass of about 3 GeV a 3% effect is observed [5]. This is because the b-quark mass suppresses gluon radiation in the same way that Bremsstrahlung is suppressed for muons compared to electrons.

In this analysis a large set of event shape observables has been employed in addition to the three-jet rate in order to extract a value of the b-quark mass from the measured ratios of the observables in b and uds induced events. The suppression of gluon radiation by the b-quark mass affects the event-shape distributions, and these variables have rather different behaviour with respect to the hadronization and next-to-leading order effects.

In the following section the analysis method is outlined, then a description of the ALEPH detector is given, followed by a summary of the data analysis. In Section 3.7 the results for the measurements of the ratio of observables in b and uds events are given, which are then used to determine the b-quark mass (Section 4). The mass measurement is summarized in Section 4.3 and the conclusions are given in Section 5.

2 The Analysis Method

As will be described in Section 4.1, the running b-quark mass enters into the theoretical prediction for the ratio

$$R_{bl}^{part} = \frac{O_b}{O_l} \quad , \tag{1}$$

where O_b (O_l) are infrared and collinear safe observables at parton level (quarks and gluons, *part*) for Z decays into b or light ($l = uds$) quark pairs. The measured ratio R_{bl}^{meas} can be related to the ratio at the parton level via the following formula :

$$R_{bl}^{meas} = \frac{R_{bl}^{part} H_{b/l} D_{b/l} T_{bb,ll} P_{bb,ll} + R_{cl}^{part} H_{c/l} D_{c/l} T_{cb,ll} P_{cb,ll} + T_{lb,ll} P_{lb,ll}}{R_{bl}^{part} H_{b/l} D_{b/l} T_{bl,ll} P_{bl,ll} + R_{cl}^{part} H_{c/l} D_{c/l} T_{cl,ll} P_{cl,ll} + 1} \quad . \tag{2}$$

Here $H_{b/l} = Had_b/Had_l$ is the ratio of hadronization corrections for b and light quark events, equivalently $D_{b/l} = Det_b/Det_l$ is the ratio of detector corrections for the two flavour samples, taking into account the effects of finite detector resolution and acceptance. $T_{xy,ll} = Tag_{xy}/Tag_{ll}$ is a ratio of tagging corrections, which correct for biases introduced by the flavour tag, ie., the selection criteria for the samples enriched in b- and uds-quarks. Here Tag_{xy} is the ratio of the observable before and after the tag, with x being the true flavour of the event, and y the tagged one. Finally, $P_{xy,ll} = \mathcal{P}_{xy}/\mathcal{P}_{ll}$ is a ratio of purities, where $\mathcal{P}_{xy}$ stands for the probability that an event with x as primary flavour is tagged as a y flavour event. All these correction factors and purities are obtained from Monte Carlo (MC). Since mainly ratios of corrections are involved, it can be expected that certain systematic uncertainties cancel out.

R_{bl}^{part} is extracted from the relationship (2) and finally corrected for the contribution of anomalous triangle diagrams [20], in order to relate R_{bl}^{part} to R_{bd}^{part} for which the perturbative calculations have been performed. The triangle contributions cancel out in the second ratio. However, they give a contribution of the order of 0.2% to the first.

As observables O_x the following variables have been studied :

- The rate of three-jet events, where the jets are defined by the Durham clustering and E-recombination scheme [17], for a fixed value of the resolution parameter $y_{cut} = 0.02$. It has been shown in Ref. [5] that this choice of y_{cut} represents a good compromise between the actual size of the mass effect to be measured, and the size of systematic uncertainties, in particular the hadronization uncertainties.

- The first and second moments of the event shape variables Thrust T, C-parameter C , $y3$, Total and Wide Jet Broadening, B_T and B_W. The definitions of the observables can be found, eg., in [18, 19] and references therein. Moments have been chosen instead of distributions because of the better statistical accuracy with which the perturbative predictions could be evaluated by MC integration. Even higher moments would give smaller hadronization uncertainties, however, the NLO corrections get typically larger and the overall mass effects fall below the 3% level.

3 Data Analysis

3.1 The ALEPH Detector

The ALEPH detector is described in detail elsewhere [10, 11]. Briefly, at the core of the tracking system is a silicon strip vertex detector (VDET). This has two layers, at average radii of 6.5 and 11.3 cm, each providing measurements in both the r-ϕ and r-z views. The spatial resolution for r-ϕ coordinates is 12 μm and varies between 12 and 22 μm for z coordinates, depending on the track polar angle. The angular coverage of the VDET is $|\cos\theta| < 0.85$ for the inner layer and $|\cos\theta| < 0.69$ for the outer layer. The VDET lies within a small cylindrical drift chamber (ITC), which measures up to eight coordinates per track in the r-ϕ view, with a resolution of 150 μm. The ITC is in turn enclosed in a large time projection chamber (TPC), lying between radii of 30 and 180 cm. This provides up to 21 three-dimensional coordinates per track, with resolutions

in the r-ϕ and r-z views of 180 μm and 1-2 mm, respectively. The three tracking detectors are surrounded by a superconducting solenoid producing a magnetic field of 1.5 T.

For charged tracks with two VDET coordinates, a transverse momentum resolution of $\Delta p_T/p_T = 6 \times 10^{-4} p_T \oplus 0.005$ (p_T in GeV/c) is achieved. The impact parameter resolution is $25 \oplus 95/p$ μm (p in GeV/c) in both the r-ϕ and r-z views.

An electromagnetic calorimeter (ECAL) and a hadron calorimeter (HCAL) are used to measure the energies of neutral and charged particles over almost the full 4π solid angle. The ECAL is a lead/wire-chamber sandwich operated in proportional mode and is read out via projective towers subtending typically $0.9^\circ \times 0.9^\circ$. A relative energy resolution of $0.18/\sqrt{E}$ (E in GeV) is obtained. The HCAL uses the iron return yoke as absorber and has an average depth of 1.2 m. Hadronic showers are sampled by 23 planes of streamer tubes, which induce an analog signal on pads arranged in projective towers of approximately $3.7^\circ \times 3.7^\circ$. In association with the ECAL, the HCAL also provides a measurement of the energy of charged and neutral hadrons with a relative resolution of $0.8/\sqrt{E}$ (E in GeV).

Muon chambers consisting of two double layers of streamer tubes surround the HCAL. Electrons and photons can be identified using the ECAL, whilst muons are seen as tracks giving a series of hits on digitally readout strips in the HCAL and muon chamber streamer tubes.

Combining the information of all subdetectors, an energy-flow algorithm [12] provides a measurement of the total energy and a list of charged and neutral reconstructed objects, called *energy-flow objects*, with measured momentum vectors and information on particle type.

3.2 Event Selection

In this analysis data taken at the Z peak in 1994 are used. First a hadronic selection is applied. Charged particle tracks are selected that have at least four measured space coordinates from the TPC, a polar angle in the range $20^\circ < \theta < 160^\circ$, and a transverse momentum with respect to the beam direction of $p_\perp > 0.2$ GeV/c. In addition, the closest radial distance of approach of the extrapolated track to the beam axis, d_0, is required to be less than 2 cm, and the z-coordinate of the point of closest radial approach, z_0, is required to be less than 10 cm. Using these selected charged tracks, the total charged energy $E_{ch} = \sum_i \sqrt{p_i^2 + m_\pi^2}$ is computed. Neutral energy-flow objects are kept if their polar angle with respect to the beam axis is in the range $11.5^\circ < \theta < 168.5^\circ$.

Events are selected that have at least five selected charged particle tracks, $E_{ch} > 15$ GeV, and $|cos\theta_T| < 0.7$, where θ_T is the polar angle of the thrust axis, computed from all charged and neutral particles. This last cut ensures that the events are well contained within the VDET. According to the MC simulation, this cut, when combined with the basic hadronic event selection, is about 62% efficient. Non-hadronic background, which is dominated by $\tau^+\tau^-$ events, represents 0.3% of this sample. After the selection, a sample of 1.1 million hadronic events remain for further analysis. The observables described in Section 2 are computed taking all selected charged and neutral energy-flow objects.

The analysis also uses 3.34 million simulated hadronic events produced with a generator based on the JETSET 7.4 parton shower model [13]. The production rates, decay modes and lifetimes of heavy hadrons are adjusted to agree with recent measurements, while heavy quarks are fragmented

using the Peterson model [14]. Detector effects are simulated using the GEANT package [15]. The MC events are reweighted in order to reproduce the measured values for the gluon splitting rates into $b\bar{b}$ and $c\bar{c}$ pairs [16].

3.3 Flavour Tagging

For the flavour tagging the events are first divided into two hemispheres using the plane perpendicular to the thrust axis, and then a b- and a $l(=uds)$-tag is applied to both hemispheres.

3.3.1 *b*-tag

The b-tag, ie., the criteria used to select b events, follows closely the approach described in detail in Ref. [21]. Briefly, b hadrons are tagged by their long lifetime detected by the VDET. To improve rejection of c hemispheres, the lifetime tag is combined with a further tag exploiting the b/c hadron mass difference. In contrast to [21], where for each hemisphere a main vertex was constructed, here only one main vertex for the event is used.

3.3.2 *l*-tag

In order to obtain a good efficiency and high purity for tagging light quark hemispheres, five variables per hemisphere are combined in order to construct a discriminant variable. The five variables are :

- The probability that all tracks in a hemisphere come from the primary vertex (cf. [21]).
- The momentum of the fastest particle in the hemisphere.
- The total visible energy in the hemisphere.
- The squared transverse momentum of a π_{soft} candidate with respect to its jet direction [22].
- The transverse momentum with respect to its jet of an identified lepton (if any). The lepton identification is based on the method described in [23].

The purity distributions $N(uds)/N(udscb)$ for each variable are taken from MC and parametrized with simple functions. A discriminant variable x is defined as

$$x = \frac{\prod_{i=1}^{5} \mathcal{P}_i}{\prod_{i=1}^{5} \mathcal{P}_i + \left[\prod_{i=1}^{5}(1-\mathcal{P}_i)\right]\left(\frac{\mathcal{P}_{uds}}{1-\mathcal{P}_{uds}}\right)} \quad , \tag{3}$$

where $\mathcal{P}_i$ is the purity for the i-th variable, and $\mathcal{P}_{uds}$ is the initial uds purity of the sample. The variable x represents the purity in the vicinity of the cut, in the ideal situation where no correlation between variables is present.

3.3.3 Tag Performance

In Figs. 1 and 2 the distributions of the tag variables for the b- and the l-tag are shown. In the relevant regions, namely at large values, good agreement between data and MC is observed. For each tag, the values of the tag variables found in both hemispheres are taken to define a criterion for the event tag. In particular, it is required that the sum of the two hemisphere tag variables exceed a certain cut value b_{cut}, l_{cut}. Furthermore, ambiguous events are rejected, for which both the b- and the l-tag are successful. This reduces the overall event selection efficiency to about 60%.

The cuts are chosen such that the overall corrections factors remain within a few percent, obtaining at the same time good efficiencies and reasonable purities. The purities and efficiencies for the cut values $b_{cut} = 1.2, l_{cut} = 0.8$ are reported in Table 1, together with the statistical errors. In the data 231 051 events are tagged by the b-tag, and 736 530 events by the l-tag.

3.4 Detector and Tagging Corrections

The observables have to be corrected for detector effects, such as finite acceptance and resolution, by computing the observables before and after the detector simulation and imposing the same track and event selection cuts as for the data, without applying any flavour tag. The ratios of the observables are computed for each true flavour, ie., the quark flavour of the primary decay products of the Z boson. The ratios of detector corrections $D_{b/l}$ as defined in Section 2 are found to be typically of the order of 0.95.

The flavour tag can introduce a bias to the measured observables. It is estimated by computing the observable before and after applying the tag to the MC sample which passed the event selection cuts, for every true and tagged flavour. For example, in case of the three-jet rate and the second moment of the Wide Jet Broadening a correction of $T_{bb,ll} = 0.96$ is found.

3.5 Hadronization Corrections

The perturbative predictions are corrected for hadronization effects by computing the relevant observables at parton and at hadron level. The JETSET parton shower model together with the Lund string fragmentation scheme is employed for this purpose. The model parameters have been taken from [18], with the exception that final state radiation is not included in the simulation. Mass effects are introduced by kinematic constraints to the phase space at each parton branching in the shower evolution. The default value of m_b employed by this program is 5 GeV. Ten million events have been generated and analyzed. The corrections have been computed for each flavour individually.

Another ten million events have been generated with the PYTHIA 5.7 generator [13] with and without initial and final state photon radiation. The radiation corrections deviate from unity by less than 1%.

The ratios of hadronization corrections, $H_{b/l}$, (including also radiation effects) are listed in Table 3. The corrections are rather sizeable for almost all the observables, in most cases they are of the same size or larger than the expected mass effect. Only the three-jet rate and the first two

moments of the y_3 distribution have corrections at the 1% level. However, these three variables are highly correlated.

Taking only variables which are not too much correlated and with hadronization effects of less than 10%, one remains with the three-jet rate and the second moment of B_W. Therefore only these two variables have been studied further.

3.6 Systematic Errors

A good description by the MC of relevant quantities such as purities and tagging biases is essential for this analysis. Systematic uncertainties can arise from imperfections of the implementation of the physics processes as well as from deficiencies in the description of the detector performance. In order to study possible biases, the cut variables for the two tags have been varied over a wide range, corresponding to changes in the b purity $\mathcal{P}_{bb}$ from 80.4% to 90.0% and in the uds purity $\mathcal{P}_{ll}$ from 80.9% to 86.1%. When cutting very hard on the tagging variables in order to obtain purities above 90%, the overall corrections get rather large, up to 20%, which is clearly much larger than the mass effect. Therefore only cut variations have been considered which give an overall correction of less than two times the mass effect to be measured (0.97 for $R_{3j}^{Dur}(0.02)$ and 0.93 for B_{W_2}), hence 6% in the case of the three-jet rate and 14% for the second moment of the Wide Jet Broadening. Taking half of the range of the measured R_{bl}^{part} which is spanned by those variations, results in an error of 0.005 for $R_{3j}^{Dur}(0.02)$ and of 0.003 for B_{W_2}.

The uncertainty of the gluon splitting into heavy quark pairs propagates to an error of 0.004 for both variables.

The uncertainties from the modelling of the hadronization have been evaluated by computing the hadronization corrections with different MC generators. In a first variation of the JETSET parton shower the cut-off scale Q_0 is fixed to 4 GeV and the other parameters are retuned by fitting to global event shape and inclusive charged track distributions. This results in a mean multiplicity of four partons, which is much closer to the parton multiplicity considered in the NLO calculation. Another variation is obtained by using the matching of the first parton shower branchings of heavy quarks to the leading order (LO) matrix element including mass effects. No retuning of parameters is performed in this case. Finally, the HERWIG 5.9 [24] generator including a parton shower with subsequent cluster fragmentation has been used.

Similarly to the systematics from cut variations, the error due to the uncertainty of hadronization effects is defined as half of the range obtained for R_{bl}^{part} when using all four different MC models. The errors found are 0.012 for $R_{3j}^{Dur}(0.02)$ and 0.003 for B_{W_3}. The large error in case of the three-jet rate stems from a sizeable difference in the results found for the JETSET variation with $Q_0 = 4$ GeV and for HERWIG.

3.7 Results

In order to obtain the final values for R_{bd}^{part}, first the contributions from anomalous triangle diagrams are subtracted from the measured ratio R_{bl}^{part}, and then the error due to the finite MC statistics for the evaluation of purities, detector and tagging corrections is added to the statistical

error of the data. This statistical error from MC is obtained by evaluating the scatter of results when repeating the analysis with a large number of MC subsamples of smaller size, and then extrapolating the standard deviation thus found to the actual size of the original MC sample. Finally, the systematic errors from cut variations and gluon splitting uncertainties are added in quadrature. The results are

$$R_{3j}^{Dur}(0.02) \quad : \quad R_{bd}^{part} \;=\; 0.969 \pm 0.007(stat) \pm 0.008(syst) \pm 0.012(had)$$

$$B_{W_2} \quad : \quad R_{bd}^{part} \;=\; 0.928 \pm 0.004(stat) \pm 0.005(syst) \pm 0.003(had)$$

The results for all the other observables can be found in Table 3, with statistical errors only. The result for the three-jet rate is in good agreement with the one of Ref. [5].

4 Extraction of the *b*-Quark Mass

4.1 Theoretical Predictions

In general the NLO prediction for R_{bd}^{part} as a function of the observable O and the b-quark mass is of the form

$$R_{bd}^{part}(O) = 1 + r_b(\mu)\left(b_0(r_b(\mu), O) + \frac{\alpha_s(\mu)}{2\pi} b_1(r_b(\mu), O)\right) \quad , \tag{4}$$

where $r_b(\mu) = m_b^2(\mu)/M_Z^2$, and $m_b(\mu)$ is the running b-quark mass as defined in the $\overline{\rm MS}$ renormalization scheme at the renormalization scale μ. The ratio can be expressed also in terms of the pole mass M_b, namely

$$R_{bd}^{part}(O) = 1 + r_b^P\left(b_0^P(r_b^P, O) + \frac{\alpha_s(\mu)}{2\pi} b_1^P(r_b^P, O)\right) \quad , \tag{5}$$

with $r_b^P = M_b^2/M_Z^2$. The two predictions are equivalent at this order. The coefficient functions $b_{0,1}$ for the two schemes can be related to each other by expressing the pole mass in terms of the running mass, ie.,

$$r_b^P = r_b(\mu)\left[1 + \frac{\alpha_s(\mu)}{2\pi}\left(\frac{16}{3} - 4\ln r_b(\mu) + 4\ln\frac{\mu^2}{M_Z^2}\right)\right] \quad . \tag{6}$$

The coefficient functions for the three-jet rate have been computed in Ref. [1]. For all the other variables they have been obtained using the MC generators ZBB4 [4, 25] and EVENT [26]. ZBB4 allows to integrate the fully differential NLO matrix elements including mass effects, whereas EVENT contains the massless expressions [27]. The latter has been extensively employed at LEP for the calculations of the NLO predictions of event shapes used for the measurements of the strong coupling constant. The differential cross sections for any infrared and collinear safe observable O for either b or d primary quarks in e^+e^- annihilation can be written as

$$\frac{1}{\sigma_{b,d}^{tot}}\frac{d\sigma}{dO} = \frac{\alpha_s}{2\pi} A_{b,d}(O) + \left(\frac{\alpha_s}{2\pi}\right)^2 B_{b,d}(O) \quad . \tag{7}$$

Here $\sigma_{b,d}^{tot}$ is the total cross section for either b or d quark production. The functions A_b, B_b are computed with ZBB4 for fixed values of the b-quark mass in the pole mass scheme, whereas A_d

and B_d are obtained from EVENT. Taking the ratio and expanding up to NLO, the following relationships can be found :

$$r_b^P b_0^P = \frac{A_b}{A_l} - 1 \quad , \tag{8}$$

$$r_b^P b_1^P = \frac{B_b A_l - B_l A_b}{A_l^2} \quad . \tag{9}$$

In order to get the functional dependence of $b_{0,1}^P$ on the b-quark mass, first the coefficients A_b and B_b have been computed in very high statistic runs for values of $M_b = 1, 2, 3, 4, 5, 6, 10, 20$ GeV, and then expressions (8) and (9) have been fitted over the relevant range of 3 to 6 GeV using parametrisations of the type $c_1 + c_2 r_b^P + c_3 \ln r_b^P$. This parametrisation follows closely the one used in [1].

In Figs. 3 and 4 examples of these fits are shown for the first moment of Thrust and the second moment of the Wide Jet Broadening. With these parametrisations it is possible to estimate the actual quark mass effects in leading order and its next-to-leading order corrections. In Table 2 a list of these LO and NLO terms is given for all variables and for both the running and the pole mass scheme. They have been evaluated for a b-quark mass of 3 GeV in the former and 5 GeV in the latter case. It is found that for certain observables such as the jet broadening variables the mass effect is rather large. However, also the NLO corrections can be sizeable, as in the case of the second moment of Thrust and the first moment of the Wide Jet Broadening. For such critical variables it would be definitely necessary to compute also the NNLO contributions in order to obtain a reliable perturbative prediction. The NLO corrections for the second moment of the Wide Jet Broadening and the three-jet rate are of acceptable relative size needed for a sensible extraction of the b-quark mass. Finally, it can be observed that the NLO contributions relative to the LO terms are quite different for most of the observables when using either the running or the pole mass scheme, which indicates that the still un-computed higher order corrections might be very different in these two schemes.

Taking the predictions as obtained above, the running b-quark mass has been determined from the measured ratio R_{bd}^{part} for all the observables. The results are listed in Table 3. A rather large spread of mass values is found, and in general high masses with respect to the expected value of around 3 GeV are obtained. The origin of the spread is not clear yet. However, it should be remembered that most of the variables suffer from very large hadronization corrections, and in addition for some of them the NLO perturbative contributions are large. These two effects might well lead to yet uncontrollable biases.

4.2 Systematic Errors

For the two cases of three-jet rate and second moment of the Wide Jet Broadening (B_{W_2}) the systematic errors from the R_{bd}^{part} measurement have been propagated to the error of the extracted mass, and in addition further sources of systematic uncertainties have been studied.

The effects of uncalculated higher order terms are typically estimated by a change in the renormalization scale. For the central values $\mu = M_Z$ has been employed, and as systematic error half of the range of mass values is taken which is found when varying μ from $0.1 M_Z$ to $2 M_Z$. This results in a scale error of 200 MeV when using the three-jet rate, and 118 MeV when using B_{W_2}.

Another way of estimating higher order effects is given by extracting first the pole mass from the perturbative expression in the pole mass scheme, then translating that result into a running quark mass $m_b(m_b)$ at the b-mass scale, and finally running this mass up to the M_Z scale, using the relation

$$r_b(\mu) = r_b(M_Z) \left(\frac{\alpha_s(M_Z)}{\alpha_s(\mu)} \right)^{\frac{-4\gamma_0}{\beta_0}} \quad , \tag{10}$$

where $\alpha_s(\mu) = \alpha_s(M_Z)/(1 + \alpha_s(M_Z)\beta_0 \ln(\mu^2/M_Z^2)/(4\pi))$, $\beta_0 = 11 - 2n_f/3$, $n_f = 5$ and $\gamma_0 = 2$. At NLO the two methods of mass extraction are equivalent, however, the sensitivity to higher order contributions is different for the two schemes, which can then lead to different results. In case of the three-jet rate, a downward shift in the mass of -372 MeV is found when using the pole mass, and for B_{W_2} a shift of -57 MeV is observed. The behaviour of the extracted running and pole masses as a function of the renormalization scale μ is illustrated in Fig. 5.

For the strong coupling constant the value $\alpha_s(M_Z) = 0.120$ has been used for the evaluation of the central mass values. Varying the coupling by ± 0.004 gives very small effects on the b-quark mass of about 20 MeV.

Throughout the analysis the effect of the c-quark mass has been neglected, i.e., R_{cl}^{part} has been set to 1 in Eq. (2). As a systematic check R_{cl}^{part} has been evaluated using the NLO perturbative predictions for a mass of $m_c = 1.4$ GeV. The effect on the observed b-quark mass is negligible.

4.3 Results

When defining as theoretical error the quadratic sum of the various estimates of higher order effects, the final results for the mass of the b-quark are obtained :

$$\begin{aligned}
R_{3j}^{Dur}(0.02) \quad : \quad m_b(M_Z) &= 3.04^{+0.37}_{-0.34}(stat)\,^{+0.44}_{-0.39}(syst)\,^{+0.72}_{-0.59}(had)\,^{+0.20}_{-0.42}(theo) \text{ GeV} \\
&= 3.04 \pm 0.92 \text{ GeV} \\
B_{W_2} \quad : \quad m_b(M_Z) &= 3.78 \pm 0.14(stat) \pm 0.17(syst) \pm 0.10(had)\,^{+0.12}_{-0.13}(theo) \text{ GeV} \\
&= 3.78 \pm 0.27 \text{ GeV}
\end{aligned}$$

These values can be translated into $m_b(m_b) = 4.16 \pm 1.10$ GeV, $M_b = 4.53 \pm 1.18$ GeV for $R_{3j}^{Dur}(0.02)$, and $m_b(m_b) = 5.04 \pm 0.32$ GeV, $M_b = 5.47 \pm 0.34$ GeV for B_{W_2}. The result obtained with the three-jet rate is in agreement with the one found in Ref. [5]. Using the second moment of the Wide Jet Broadening results in a somewhat higher value, with a much reduced statistical and systematic error. However, for the interpretation of this second result it should be considered that the hadronization correction in case of this observable is 9%, which is even slightly larger than the mass effect to be measured. So although the hadronization error turns out to be rather small, it could well be that there is an additional bias towards higher masses introduced by all the hadronization models which have been considered. A similar spread of measured masses has been reported in Ref.[6], where different clustering algorithms for the three-jet rate have been studied. It is known that the size of the hadronization and NLO corrections differ quite a lot between the various algorithms, which then could possibly explain the spread in the measured b-quark masses.

5 Conclusions

A large set of observables has been used in order to study the running b-quark mass from the measured ratio of the observable in b- and light quark decays of the Z boson in e^+e^- annihilation. Taking as observable the three-jet rate as defined by the Durham algorithm with $y_{cut} = 0.02$, a b-quark mass of

$$m_b(M_Z) = 3.04^{+0.37}_{-0.34}(stat)\,^{+0.44}_{-0.39}(syst)\,^{+0.72}_{-0.59}(had)\,^{+0.20}_{-0.42}(theo)\ \text{GeV} = 3.04 \pm 0.92\ \text{GeV}$$

is found, which is in agreement with recent measurements by other experiments [5, 6]. Taking also first and second moments of event shape distributions, a large spread in measured b-quark masses is found, which might be traced back to uncontrolled biases from the hadronization and/or next-to-leading order corrections. Taking the event shape distribution with the smallest hadronization correction (9%) and which is not very highly correlated with the three-jet rate, namely the second moment of the Wide Jet Broadening, a b-quark mass of

$$m_b(M_Z) = 3.78 \pm 0.14(stat) \pm 0.17(syst) \pm 0.10(had)\,^{+0.12}_{-0.13}(theo)\ \text{GeV} = 3.78 \pm 0.27\ \text{GeV}$$

is determined. This shows that statistical as well as systematic errors might be reduced when going to other variables than the three-jet rate. However, because of the still large hadronization corrections the interpretation of the result should be performed with care.

6 Acknowledgements

We would like to thank G. Rodrigo and P. Nason for providing us with the theoretical input. Furthermore we would like to thank J. Fuster and S. Marti i Garcia for many interesting discussions on the subject.

We wish to thank our colleagues from the accelerator divisions for the successful operation of LEP. It is also a pleasure to thank the technical personnel of the collaborating institutions for their support in constructing and maintaining the ALEPH experiment. Those of the collaboration not from member states thank CERN for its hospitality.

References

[1] G Rodrigo, QCD96 Montpellier, hep-ph/9609213 and Nucl. Phys. Proc. Suppl. **54A** (1997) 60.

[2] G Rodrigo, M. Bilenky, A. Santamaria, Phys. Rev. Lett. **79** (1997) 193.

[3] W. Bernreuther, A. Brandenburg, P. Uwer, Phys. Rev. Lett. **79** (1997) 189.

[4] P. Nason, C. Oleari, Phys. Lett. **B407** (1997) 57.

[5] P. Abreu et al., DELPHI Collab., Phys. Lett. **B418** (1998) 430.

[6] A. Brandenburg et al., hep-ph/9905495, (1999), submitted to Phys. Lett. B.

[7] G. Abbiendi et al., OPAL Collab., CERN-EP/99-045, (1999), submitted to Eur. Phys. J. C.

[8] K. Abe at al., SLD Collab., Phys. Rev. **D59** (1999) 12002.

[9] C. Caso et al., Particle Data Group, Eur. Phys. J. **C3** (1998) 1.

[10] D. Decamp et al., ALEPH Collab., Nucl. Instrum. Methods **A294** (1990) 121.

[11] G. Batignani et al., conference record of 1991 IEEE Nuclear Physics Symposium, Santa Fe, USA, Vol. 1, p. 438.

[12] D. Buskulic et al., ALEPH Collab., Nucl. Instrum. Methods **A360** (1995) 481.

[13] T. Sjöstrand, Comp. Phys. Comm. **82** (1994) 74.

[14] C. Peterson et al., Phys. Rev. **D27** (1983) 105.

[15] R. Brun et al., CERN DD/EE/84-1 (1987).

[16] D. Abbaneo et al., LEP Heavy Flavour Working Group, LEPHF/98-01, ALEPH Note 98-062, PHYSIC 98-027, 1998.

[17] S. Catani et al., Phys. Lett. **B269** (1991) 179.
N. Brown, J. Stirling, Z. Phys. **C53** (1992) 629.

[18] R. Barate et al., ALEPH Collab., Phys. Rep. **294** (1998) 1.

[19] S. Catani, G. Turnock, B.R. Webber, Phys. Lett. **B295** (1992) 269.

[20] K. Hagiwara, T. Kuruma, Y. Yamada, Nucl. Phys. **B358** (1991) 80.
G. Rodrigo, private communication.

[21] R. Barate et al., ALEPH Collab., Phys. Lett. **B401** (1997) 150.

[22] D. Buskulic et al., ALEPH Collab., Phys. Lett. **B352** (1995) 479.

[23] D. Buskulic et al., ALEPH Collab., Nucl. Instr. Methods **A346** (1994) 461.

[24] G. Marchesini, B.R. Webber, G. Abbiendi, I.G. Knowles, M.H. Seymour and L. Stanco, Comp. Phys. Comm. **67** (1992) 465.

[25] P. Nason, private communication, 1998.

[26] Z. Kunszt, Paolo Nason, private communication.
G. Altarelli, R. Kleiss, C. Verzegnassi, *Z Physics at LEP1*, CERN Yellow Report 89-08, vol.1, p.373.

[27] R.K. Ellis, D.A. Ross, A.E. Terrano, Nucl. Phys. **B178** (1981) 421.

ϵ_b	$\mathcal{P}_{bb}$	$\mathcal{P}_{cb}$	$\mathcal{P}_{lb}$
86.73 ± 0.05	83.37 ± 0.06	13.80 ± 0.05	2.83 ± 0.02
ϵ_l	$\mathcal{P}_{ll}$	$\mathcal{P}_{cl}$	$\mathcal{P}_{bl}$
96.70 ± 0.02	83.43 ± 0.03	14.47 ± 0.03	2.10 ± 0.01

Table 1: Efficiencies $\epsilon_{b,l}$ and purities as defined in Section 2 for the b-and l-tags, for the cut values $b_{cut} = 1.2, l_{cut} = 0.8$. The errors are statistical. All numbers are in percent.

O	LO (run)	NLO (run)	LO (pol)	NLO (pol)
T_1	3.6	1.9	7.6	-0.7
T_2	1.7	3.2	4.3	3.6
C_1	4.4	2.2	9.1	-1.1
C_2	2.1	3.9	5.2	4.3
y_{3_1}	3.2	0.7	7.1	-2.1
y_{3_2}	1.5	0.3	3.2	-0.7
B_{T_1}	11.7	0.6	18.8	-7.4
B_{T_2}	3.6	11.2	8.0	12.3
B_{W_1}	11.7	-8.5	18.8	-18.3
B_{W_2}	3.6	1.6	8.0	-1.3
$R_{3j}^{Dur}(0.02)$	2.0	0.5	5.6	-0.4

Table 2: Table of the leading (LO) and next-to-leading (NLO) order contributions to $1 - R_{bd}^{part}$ in percent, for the running mass (run) and the pole mass (pol) scheme. The contributions are evaluated for a running (pole) mass of 3 (5) GeV. The strong coupling α_s is set to 0.12.

O	$H_{b/l}$	R_{bl}^{meas}	R_{bd}^{part}	$m_b(M_Z)$
T_1	1.142	1.038 ± 0.002	0.904 ± 0.003	4.48 ± 0.09
T_2	1.139	1.023 ± 0.005	0.901 ± 0.006	4.84 ± 0.20
C_1	1.175	1.051 ± 0.002	0.890 ± 0.002	4.41 ± 0.06
C_2	1.181	1.047 ± 0.003	0.887 ± 0.004	4.69 ± 0.12
y_{3_1}	1.029	0.987 ± 0.005	0.942 ± 0.007	3.89 ± 0.28
y_{3_2}	0.990	0.982 ± 0.009	0.981 ± 0.015	$3.51^{+1.50}_{-0.95}$
B_{T_1}	1.302	1.076 ± 0.001	0.832 ± 0.001	3.94 ± 0.03
B_{T_2}	1.333	1.088 ± 0.003	0.825 ± 0.003	3.57 ± 0.06
B_{W_1}	1.142	1.043 ± 0.002	0.903 ± 0.002	4.74 ± 0.05
B_{W_2}	1.093	1.035 ± 0.001	0.928 ± 0.004	3.78 ± 0.14
$R_{3j}^{Dur}(0.02)$	0.989	0.991 ± 0.005	0.969 ± 0.007	$3.04^{+0.37}_{-0.34}$

Table 3: Table of the ratio of hadronization corrections $H_{b/l}$, the measured ratio R_{bl}^{meas}, the corrected ratio R_{bd}^{part} and the extracted running b-quark mass $m_b(M_Z)$, for the flavour tagging cuts $b_{cut} = 1.2, l_{cut} = 0.8$. The errors are statistical only. The statistical error of R_{bd}^{part} includes the statistical error from the MC.

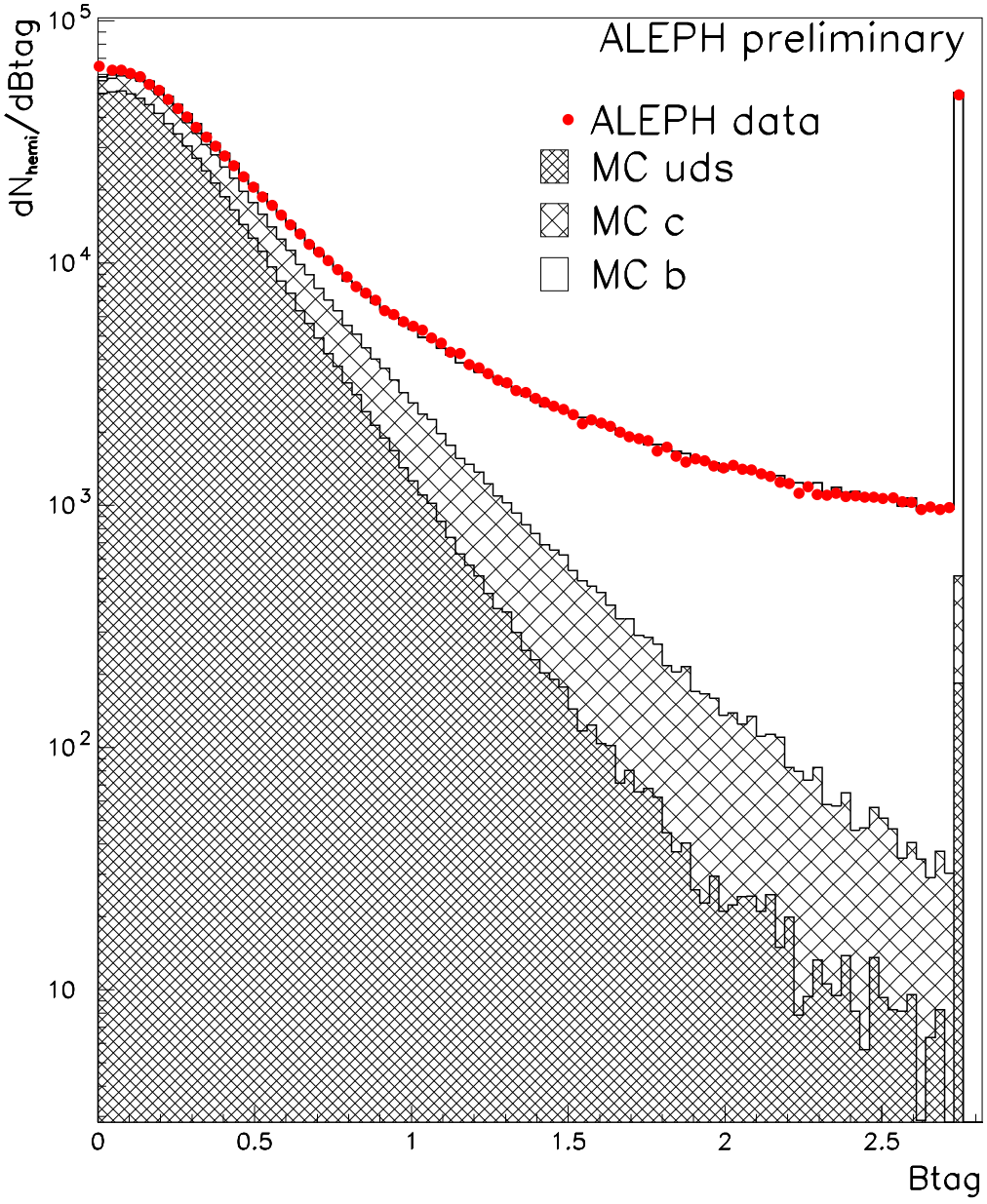

Figure 1: Distribution of the b-tag variable which is a combination of lifetime and mass information for data hemispheres and for Monte Carlo b, c and uds hemispheres. The Monte Carlo has been normalized to the same number of events as the data. The last bin includes overflow entries.

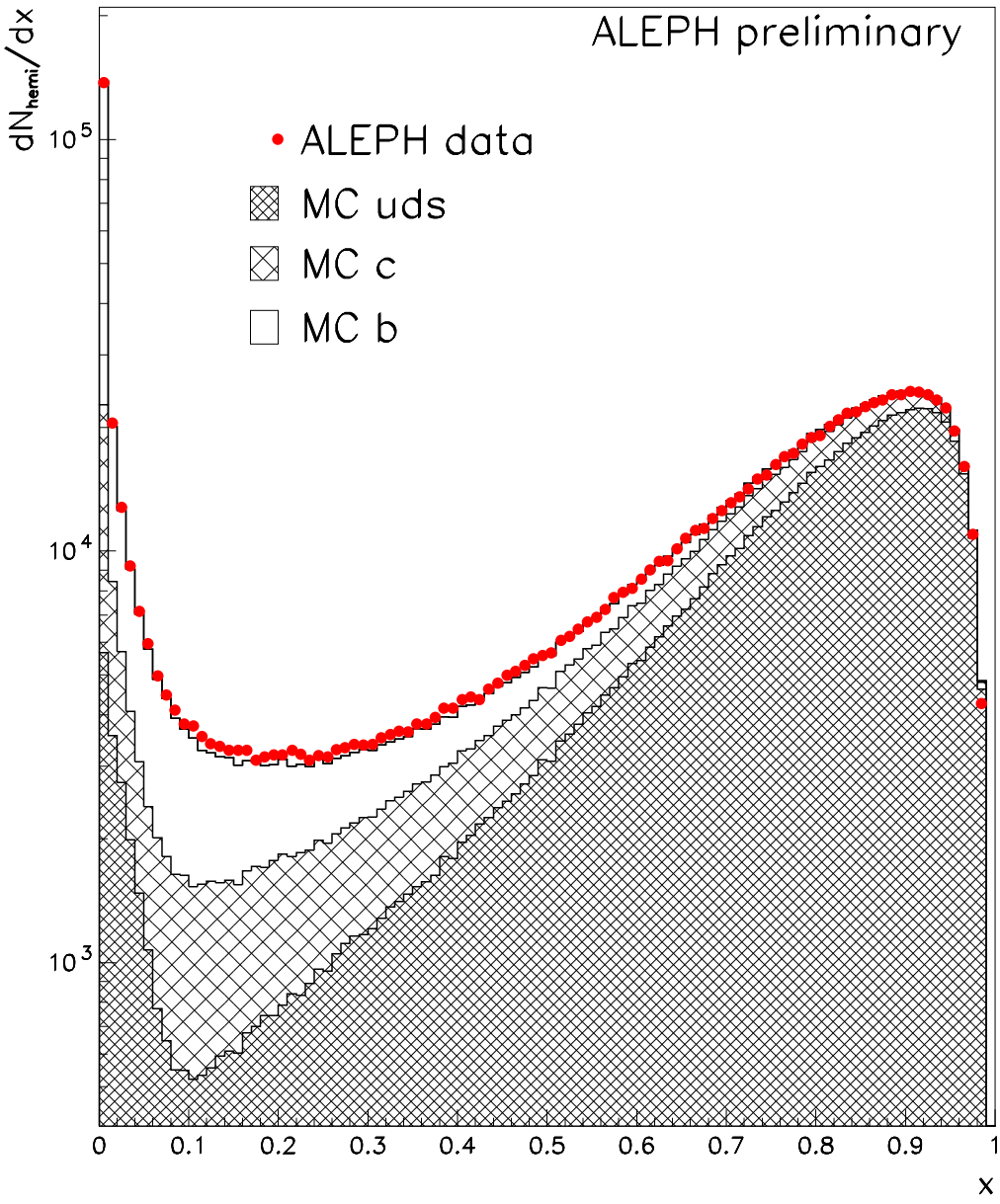

Figure 2: Distribution of the l-tag discriminant variable x for data hemispheres and for Monte Carlo b, c and uds hemispheres. The Monte Carlo has been normalized to the same number of events as the data.

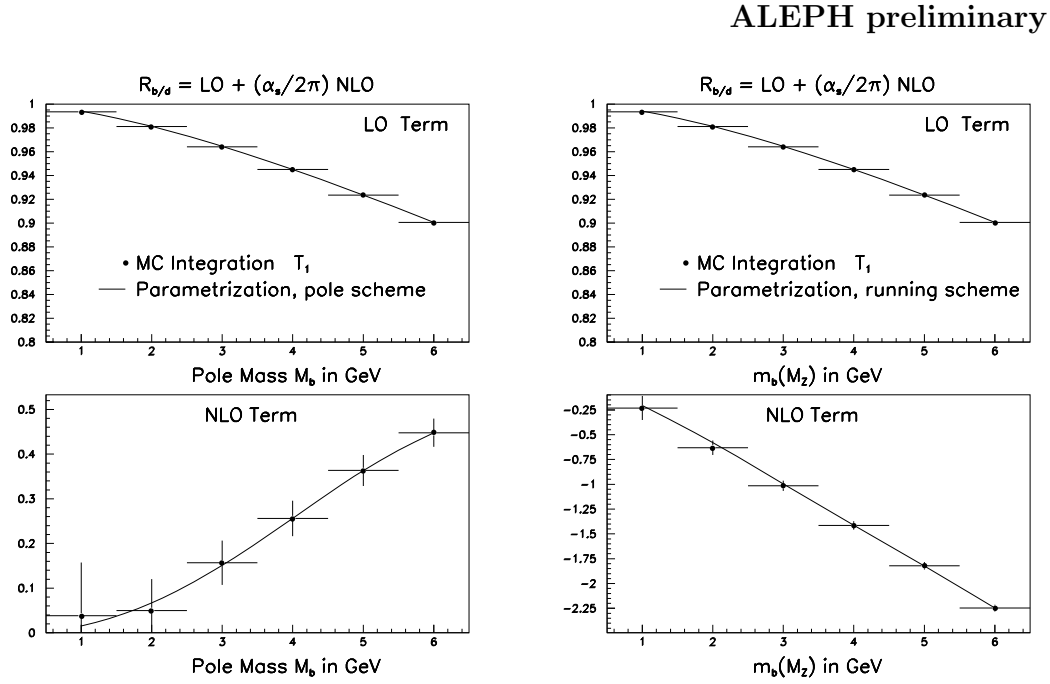

Figure 3: Parametrisations of the b-quark mass dependence for the coefficient functions b_0 (top) and b_1 (bottom) in the pole mass (left) and running mass scheme (right) for the first moment of (1-Thrust).

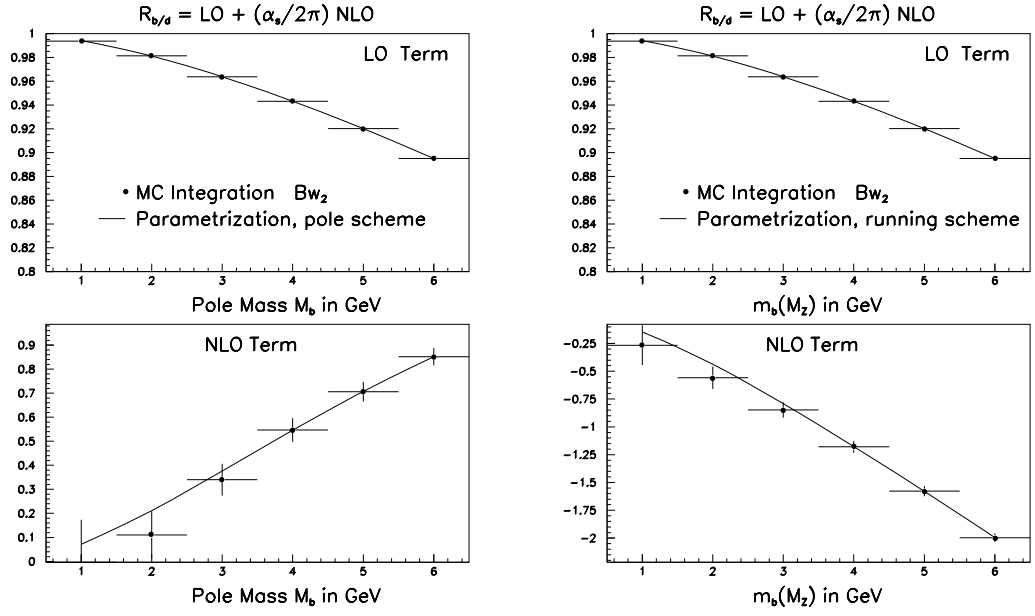

Figure 4: Parametrisations of the b-quark mass dependence for the coefficient functions b_0 (top) and b_1 (bottom) in the pole mass (left) and running mass scheme (right) for the second moment of the Wide Jet Broadening.

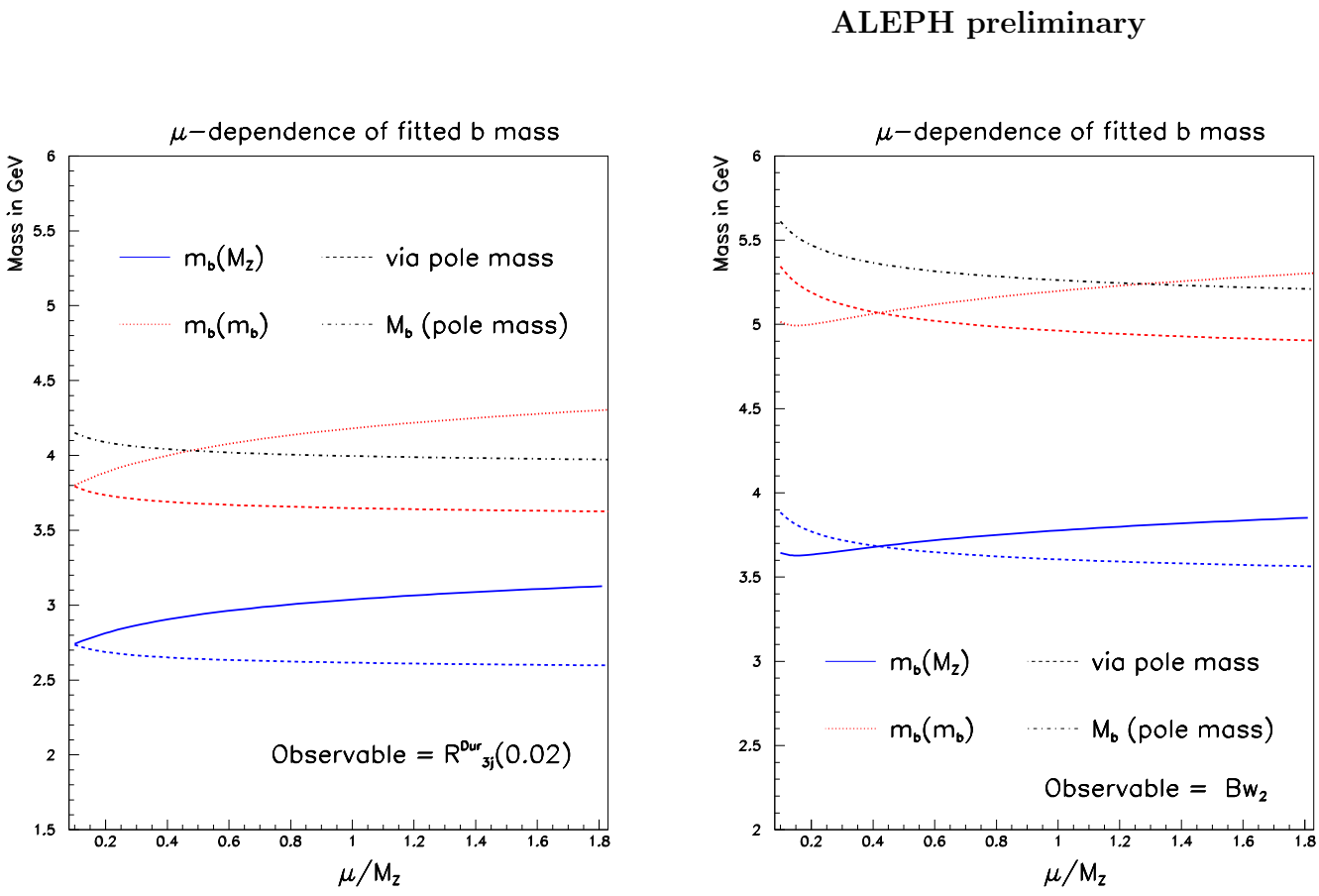

Figure 5: Renormalization scale dependence for the extracted running mass at the scales M_Z and m_b and the pole mass, for the three-jet rate (left) and the second moment of the Wide Jet Broadening (right).